PLANT SCIENCES

m^{6}A RNA demethylase AtALKBH9B promotes mobilization of a heat-activated long terminal repeat retrotransposon in *Arabidopsis*

Wenwen Fan[1,2]†, Ling Wang[1,2]†, Zhen Lei[1,2]†, Hui Li[1,2]†, Jie Chu[1,2]*†, Mengxiao Yan[3], Yuqin Wang[3], Hongxia Wang[1,2,3], Jun Yang[1,2,3], Jungnam Cho[1,2,4,5]*

Transposons are mobile and ubiquitous DNA molecules that can cause vast genomic alterations. In plants, it is well documented that transposon mobilization is strongly repressed by DNA methylation; however, its regulation at the posttranscriptional level remains relatively uninvestigated. Here, we suggest that transposon RNA is marked by m^{6}A RNA methylation and can be localized in stress granules (SGs). Intriguingly, SG-localized AtALKBH9B selectively demethylates a heat-activated retroelement, *Onsen*, and thereby releases it from spatial confinement, allowing for its mobilization. In addition, we show evidence that m^{6}A RNA methylation contributes to transpositional suppression by inhibiting virus-like particle assembly and extrachromosomal DNA production. In summary, this study unveils a previously unknown role for m^{6}A in the suppression of transposon mobility and provides insight into how transposons counteract the m^{6}A-mediated repression mechanism by hitchhiking the RNA demethylase of the host.

INTRODUCTION

Transposable elements (TEs or transposons) are DNA molecules that can move from one place to another and are widespread in most eukaryotic genomes (*1*–*3*). Two classes of transposons have been identified: class I RNA transposons that move by a "copy-and-paste" mechanism through an RNA intermediate and class II DNA transposons that move by a "cut-and-paste" mechanism (*1*, *4*). Because of their potentially adverse effects on host genomes, most transposons are strongly repressed by epigenetic mechanisms, including DNA methylation and histone modifications (*5*–*9*). Despite their strong epigenetic repression, transposons can be activated by environmental challenges, which thereby bring about genetic diversity and adaptive changes of evolution (*1*, *10*, *11*). For example, a Ty1/Copia-like retrotransposon of *Arabidopsis* called *Onsen* can be transcriptionally activated by heat stress and confers heat responsiveness to genes located downstream of insertion positions (*12*, *13*).

It is well documented that *Onsen* is strongly suppressed by epigenetic pathways involving small interfering RNAs (siRNAs) (*12*, *14*, *15*). Recently, CHROMOMETHYLASE 3 (CMT3) was suggested to promote *Onsen* transcription by preventing CMT2-mediated CHH (H; A, T, or C) methylation and histone H3 lysine 9 dimethylation accumulation at *Onsen* chromatin under heat stress (*16*). Similarly, histone H1 represses the expression of *Onsen* under heat stress and is required for DNA methylation (*17*). Whereas the repression of *Onsen* at the transcriptional level by DNA methylation is very well characterized, the regulation of *Onsen* RNA at the posttranscriptional level has not been extensively investigated.

Posttranscriptional RNA modification has emerged as a critical regulatory mark relevant to a variety of RNA processes (*18*–*21*). Its study is often referred to as epitranscriptomics, analogous to epigenetics. Cellular RNAs contain at least 100 different kinds of posttranscriptional modifications, and N6-methyladenosine (m^{6}A) is the most abundant modification type present in mRNAs (*18*, *19*, *22*, *23*). In plants and other eukaryotes, m^{6}A methyltransferases catalyze RNA methylation at a highly conserved sequence motif, RRACH (R; G or A) (*24*, *25*). In *Arabidopsis*, it has been previously demonstrated that m^{6}A RNA methylation is critical for a variety of biological processes, including development, stress response, and hormone signaling (*25*–*31*). Several studies also suggested that m^{6}A RNA modification regulates TEs; in mammalian cells, for instance, the m^{6}A writer complex and reader protein YTH domain containing 1 suppress the expression of endogenous retroviruses (*32*, *33*). In contrast, methyltransferase-like protein 3 promotes the transposition of long interspersed element-1 (L1), while RNA demethylase AlkB homolog 5 (ALKBH5) inhibits L1 mobility (*34*, *35*).

The *Arabidopsis* genome contains 13 ALKBH homologous proteins (*36*), five of which exhibit a high level of similarity to ALKBH5 (*27*). To date, only two proteins, AtALKBH9B and AtALKBH10B, have been demonstrated to catalyze RNA demethylation (*27*, *37*). AtALKBH10B is involved in flowering time regulation and directly targets the transcripts of *FT*, *SPL3*, and *SPL9* (*27*, *38*). *AtALKBH9B* is distinctively expressed in the cytoplasm, unlike other RNA demethylases (*36*, *37*). Previous studies suggested that AtALKBH9B regulates infection by alfalfa mosaic virus (*37*, *39*, *40*). AtALKBH9B colocalizes with stress granule (SG) and cytoplasmic siRNA body markers (*37*), potentially implying a functional association with RNA-mediated epigenetic silencing or RNA degradation pathways. Given the similarity of replication cycles between retroviruses and retrotransposons, TEs might also be subject to RNA methylation–

[1]National Key Laboratory of Plant Molecular Genetics, CAS Center for Excellence in Molecular Plant Sciences, Shanghai Institute of Plant Physiology and Ecology, Chinese Academy of Sciences, Shanghai 200032, China. [2]University of Chinese Academy of Sciences, Beijing 100049, China. [3]Shanghai Key Laboratory of Plant Functional Genomics and Resources, Shanghai Chenshan Botanical Garden, Shanghai 201602, China. [4]CAS-JIC Centre for Excellence in Plant and Microbial Science, Shanghai 200032, China. [5]Department of Biosciences, Durham University, Durham DH1 3LE, UK.
*Corresponding author. Email: jungnam.cho@durham.ac.uk
†These authors contributed equally to this work.

mediated control; however, transposon regulation by m^{6}A RNA modification has not been explored in plants. In this work, we investigated the role of m^{6}A RNA modification in the control of transposon suppression in *Arabidopsis*, which involves TE RNA localization in SGs. Intriguingly, a specific retroelement known as *Onsen* bypasses such m^{6}A-mediated suppression by exploiting the host-encoded RNA demethylase.

RESULTS

Onsen RNA is m^{6}A-modified

It is well documented that plant transposons are massively derepressed by heat stress (*41*, *42*). Despite the strong transcriptional activation of TEs under heat, transposition events are rarely observed (*12*, *43*, *44*), implicating possible repressive mechanisms at the RNA level. Because previous studies in humans revealed the relevance of m^{6}A regulation in the control of retrotransposons, we hypothesized that plant transposons might be controlled by a similar mechanism. To test whether m^{6}A RNA modification plays a role in transposon regulation, we analyzed public datasets for m^{6}A-RNA immunoprecipitation sequencing (RIP-seq) data generated from *Arabidopsis* floral buds harvested before and after 3 hours of heat treatment (*38*). Figure 1A shows the distribution of m^{6}A enrichment across the transcribed regions, exhibiting a strong peak around the stop codon and a weaker peak at the transcriptional start site, which are consistent with the previously well-known pattern of m^{6}A (*24*, *25*, *27*, *28*, *45*). We identified almost 2000 methylated RNAs that are specifically present in the heat stress conditions (Fig. 1B) and found that these transcripts were significantly overrepresented with transposons (Fig. 1C). In addition, our analyses of the public RNA sequencing (RNA-seq) datasets generated from the same samples used in Fig. 1A also revealed that TE contains more transcripts with high m^{6}A peak numbers, including a retrotransposon family known as *Onsen* (Fig. 1D). These data collectively show that TE RNAs are more strongly modified by m^{6}A RNA methylation and partly suggest that m^{6}A RNA modification might be involved in the posttranscriptional suppression of transposon mobilization.

Onsen is a heat-activated retrotransposon and produces extrachromosomal linear DNA (eclDNA), a pre-integrational reverse-transcribed product of a DNA intermediate that inserts into a new genomic position (*12*, *42*). *Onsen* exhibited a high level of m^{6}A along its RNA, with the most prominent peak close to the start codon (Fig. 1E). The *Arabidopsis* reference genome contains eight intact elements of *Onsen*, and all these elements displayed strong m^{6}A enrichment (Fig. 1F and fig. S1). To verify the m^{6}A RNA modification of *Onsen* RNA, an Oxford Nanopore Technologies direct RNA-seq (ONT-DRS) experiment was also performed using the RNA extracted from the Col-0 seedlings heat-stressed for 24 hours. ONT-DRS is able to detect modified bases in native RNA (*46*, *47*), and our result supports the presence of m^{6}A RNA modifications in *Onsen* RNA (Fig. 1E). We further confirmed the m^{6}A levels of *Onsen* in the 24-hour heat-stressed Col-0 seedlings by quantitative polymerase chain reaction (qPCR), and a strong m^{6}A enrichment was detected in regions B and C, which is consistent with Fig. 1E (Fig. 1G). In summary, the heat-activated transposon *Onsen* is strongly marked by m^{6}A RNA methylation.

AtALKBH9B is an m^{6}A RNA demethylase that regulates *Onsen*

In search of possible regulators of *Onsen* RNA methylation, all known m^{6}A regulators were analyzed for their expression pattern under heat treatment using the public RNA-seq datasets generated from the wild-type (WT) *Arabidopsis* plants treated with 3 or 24 hours of heat stress (*38*, *44*). Most of the genes encoding m^{6}A writers, erasers, and readers were up-regulated upon heat stress (fig. S2), possibly indicating a functional association of RNA methylation and the heat stress response. Among these genes, we focused on *AtALKBH9B*, which was previously suggested to regulate viral RNAs (*37*). Because TE RNAs share several cellular characteristics in common with viral RNAs, we hypothesized that *AtALKBH9B* might also regulate *Onsen* RNA. In line with this hypothesis, the expression patterns of *AtALKBH9B* and *Onsen* during a time course of heat treatment were similar, displaying a rather slow increase and peak at 24 hours after heat stress (fig. S3).

To test whether *AtALKBH9B* is involved in *Onsen* RNA regulation, we first isolated a transfer DNA (T-DNA) insertional mutant, *atalkbh9b-1*, and generated a deletion mutant, *atalkbh9b-2*, using the CRISPR-Cas9 system (Fig. 2A and fig. S4A). The RNA levels of *Onsen* were strongly up-regulated in both mutants under heat stress (Fig. 2B), and a similar pattern was also observed in RNA-seq data generated from the heat-stressed *atalkbh9b-1* mutant (Fig. 2C). We then expressed green fluorescent protein (GFP)–tagged AtALKBH9B in the *atalkbh9b-1* mutant and were able to detect the suppression of *Onsen* RNA to the WT level (Fig. 2D). In addition, previous studies suggested that *AtALKBH9B* and *AtALKBH10B* are expressed at high levels throughout various developmental stages, while other RNA demethylases are marginally expressed (*27*). The *atalkbh10b* mutants were thus tested for *Onsen* RNA levels; however, we were not able to detect any noticeable changes, suggesting that AtALKBH10B plays a negligible role in *Onsen* RNA regulation (fig. S5). We next performed m^{6}A-RIP-qPCR experiments using the heat-stressed WT and *atalkbh9b-1* mutant seedlings. Whereas no strong difference in the m^{6}A level was observed for a nonmethylated transposon in WT and *atalkbh9b-1* (fig. S6), the m^{6}A levels of *Onsen* RNA were significantly elevated in the *atalkbh9b-1* mutant (Fig. 2E), indicating that AtALKBH9B might cause the demethylation of *Onsen* RNA. To determine whether AtALKBH9B is a direct regulator of *Onsen* RNA, we carried out RIP-qPCR experiments using the *pAtALKBH9B::AtALKBH9B-GFP* transgenic line that expresses the tagged proteins at an equivalent level to the native AtALKBH9B (fig. S4B). Figure 2F shows a substantial level of AtALKBH9B-GFP enrichment to *Onsen* RNA, while we were unable to observe any binding enrichment in the non-methylated RNAs (fig. S1, H and I). Together, these suggest that AtALKBH9B is an RNA demethylase that directly targets *Onsen* RNA.

Loss of *AtALKBH9B* results in reduced transposition of *Onsen*

Because the RNA levels of *Onsen* were increased in the *atalkbh9b* mutants, we speculated that the transpositional activity would also be increased in the *atalkbh9b* mutants. To directly determine the *Onsen* mobility, we first carried out amplification of linear extrachromosomal DNA (ALE)–qPCR experiments that can assess the pre-integrational DNA intermediate levels (*42*). Intriguingly, the eclDNA levels of *Onsen* were markedly reduced in the *atalkbh9b-*

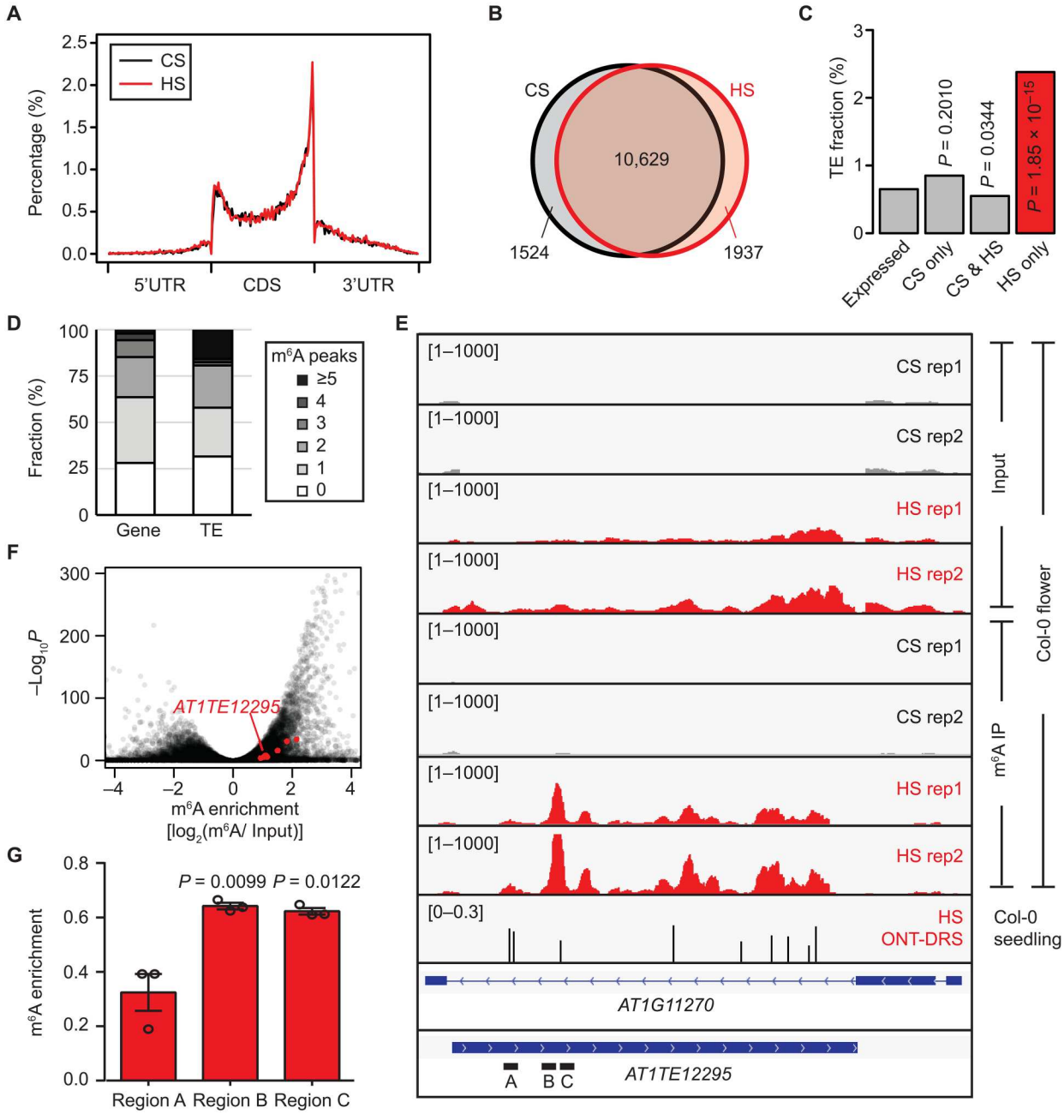

Fig. 1. *Onsen* RNA is m^{6}A-modified. (**A**) Distribution of m^{6}A RNA modification in 5′ untranslated region (5′UTR), CDS, and 3′UTR. m^{6}A enrichment was calculated for regions spanning 1% of total length. HS, heat-stressed sample (3 hours); CS, control sample. Data from the wild-type (WT) floral buds are shown. (**B**) Overlap of m^{6}A-containing transcripts in CS and HS. m^{6}A-modified transcripts were defined as those containing m^{6}A peaks detected by MACS2 at false discovery rate lower than 0.05. (**C**) Fraction of transposons in each category presented in (B). *P* values were obtained by the two-tailed Student's *t* test. (**D**) Fraction of genes (n = 15413) and transposons (n = 57) with m^{6}A RNA modifications. Genes and transposons with FPKM values greater than 5 in the heat-stressed flower sample are only considered. (**E**) m^{6}A-RIP-seq showing an *Onsen* locus and the m^{6}A sites detected by Oxford Nanopore Technologies direct RNA-seq (ONT-DRS). For ONT-DRS experiment, 1-week-old Col-0 seedlings treated with 24 hours of heat stress at 37°C were used for RNA extraction. Numbers in brackets indicate the range of coverage values (m^{6}A-RIP-seq) and fraction of m^{6}A RNA modification (ONT-DRS). Rep, biological replicate. (**F**) Volcano plot of m^{6}A enrichment. Enrichment score was determined by normalizing the m^{6}A levels to input levels. The red dots are individual *Onsen* copies, and *AT1TE12295* is marked. (**G**) Validation of m^{6}A enrichment by quantitative polymerase chain reaction (qPCR). RNA was extracted from the WT seedlings heat-stressed for 24 hours. Regions tested are as indicated in (E). *Act2* was used as an internal control. Data are shown in means ± SD from three biological replications. *P* values were obtained from the comparison to region A by the two-tailed Student's *t* test.

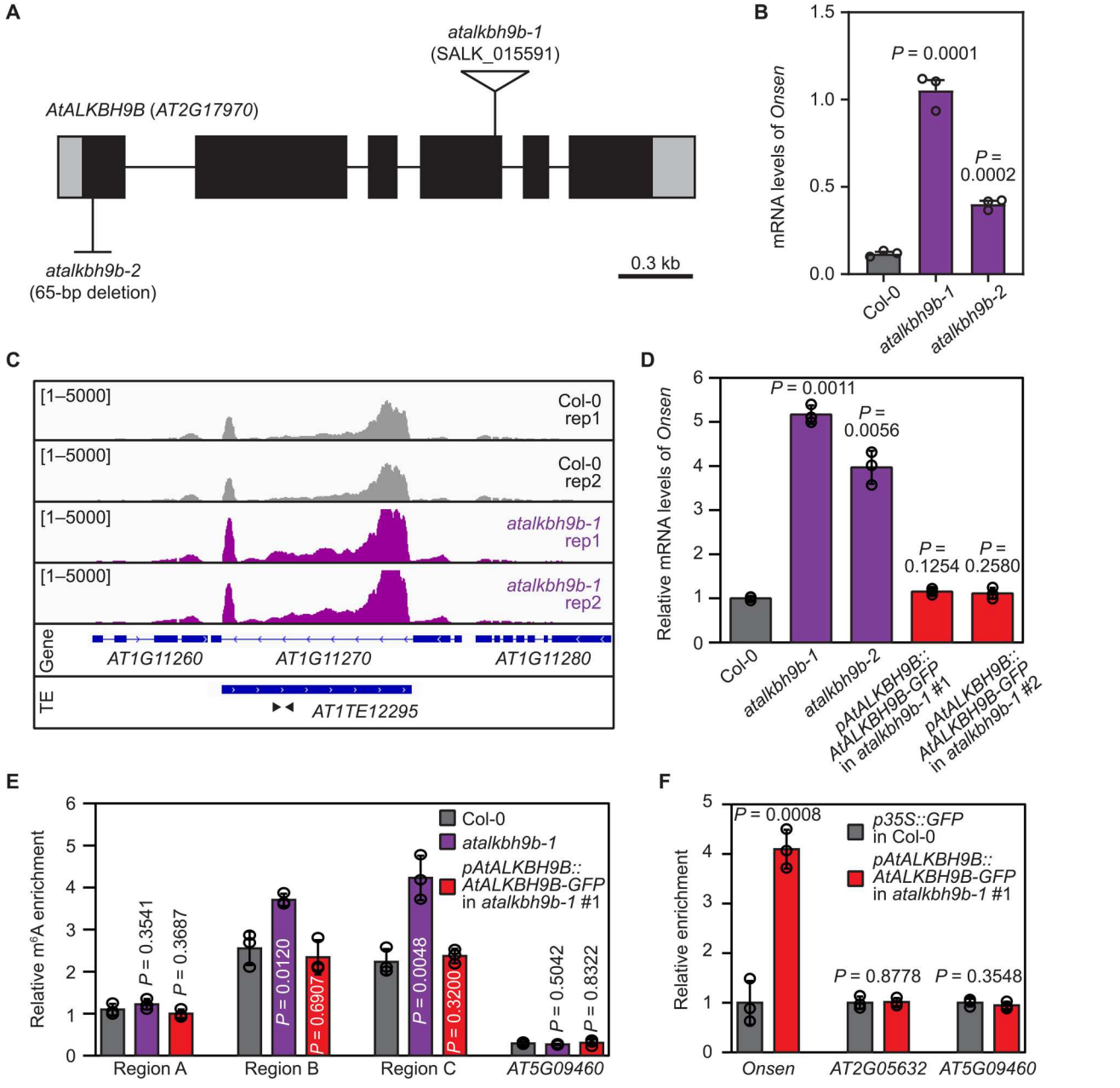

Fig. 2. *AtALKBH9B* regulates *Onsen* by directly binding to its transcripts. (**A**) Gene structure of *AtALKBH9B*. T-DNA insertion of *atalkbh9b-1* is shown as a triangle. The *atalkbh9b-2* mutant contains a large deletion of 65 base pairs (bp) in the first exon. Gray and black boxes indicate UTRs and exons, respectively. (**B**) *Onsen* RNA levels in the *atalkbh9b* mutants determined by RT-qPCR. One-week-old seedlings treated with 24 hours of heat stress at 37°C were used for RNA extraction. *Act2* was used as an internal control. Data are shown in means ± SD from three biological replications. *P* values were obtained by the two-tailed Student's *t* test. (**C**) RNA-seq of *atalkbh9b-1* showing the *Onsen* locus. Numbers in brackets indicate the range of coverage values. Arrowheads are primers used in (B), (D), and (F). (**D**) RT-qPCR for complementation assay of the *atalkbh9b-1* mutant with the *pAtALKBH9B::AtALKBH9B-GFP* construct. *Act2* was used as an internal control. Data are shown in means ± SD from three biological replications. *P* values were obtained by the two-tailed Student's *t* test. (**E**) m^6A-RIP-qPCR performed in the heat-stressed WT, *atalkbh9b-1* mutant, and a mutant complementing line. Regions are as indicated in Fig. 1E. *Act2* was used as an internal control. Data are shown in means ± SD from three biological replications. *P* values were obtained by the two-tailed Student's *t* test. (**F**) RIP-qPCR experiments using the *pAtALKBH9B::AtALKBH9B-GFP* transgenic plants used in (D). RNA was extracted from seedlings heat-stressed for 24 hours. Immunoprecipitation (IP) was performed using an anti–green fluorescent protein (GFP) antibody. Data are shown in means ± SD from three biological replications. *P* values were obtained by the two-tailed Student's *t* test.

1 mutant (Fig. 3A). Similar results were also observed in the experiments detecting the total DNA levels of *Onsen* in the heat-stressed *atalkbh9b-1* mutant (Fig. 3B). We then wanted to directly measure the insertional activity of *Onsen* in the *atalkbh9b-1* mutant, and, for this, we performed droplet digital PCR (ddPCR) experiments to quantitatively determine the copy numbers of the *Onsen* retroelement (*48*). Because the mobilization of *Onsen* is hardly detectable in the WT background, plants were grown on the medium containing α-amanitin and zebularine, which are known to enhance *Onsen* retrotransposition activity (*43*). Surviving plants after heat stress were then grown to maturity, and seeds were collected from individual plants. Plants of the subsequent generation were subjected to ddPCR without heat stress treatment to assess the genomic copies of *Onsen*. As shown in Fig. 3C, the *atalkbh9b-1* mutant generated fewer new *Onsen* copies than the WT. We then tested the *alalkbh9b-1* mutant introduced in the *nrpd1a-3* mutant background in which *Onsen* can be mobilized. Consistently, the ddPCR data revealed that the loss of *AtALKBH9B* leads to compromised retrotranspositional activity (Fig. 3D). These data indicate that *AtALKBH9B* is required for *Onsen* mobilization.

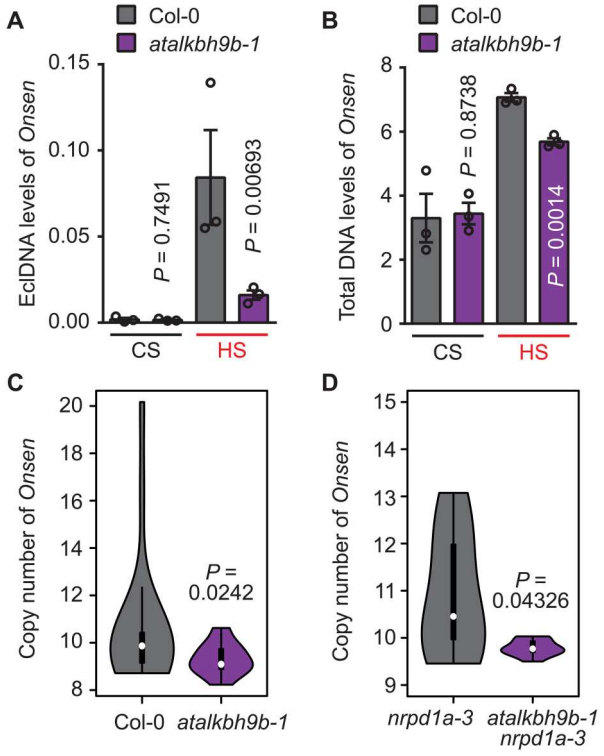

Fig. 3. Retrotransposition activity of *Onsen* is reduced in *atalkbh9b-1*. (**A** and **B**) eclDNA (A) and total DNA (B) levels of *Onsen* in the *atalkbh9b-1* mutant. Amplification of linear extrachromosomal DNA (ALE)–qPCR was performed to determine the eclDNA levels. DNA was extracted from seedlings subjected to control and 24-hour heat stress treatment. In (A), PCR-amplified *Evade* DNA was used as a spike-in control, and, in (B), *Act2* was used as an internal control. Data are shown in means ± SD from three biological replications. *P* values were obtained by the two-tailed Student's *t* test. (**C** and **D**) Copy number of *Onsen* in the progenies of WT (n = 20) and *atalkbh9b-1* (n = 19) (C) and *nrpd1a-3* (n = 10) and *nrpd1a-3 atalkbh9b-1* double mutant (n = 10) (D) that were subjected to heat stress treatment. Copy number was determined by droplet digital PCR (ddPCR) using *CBF2* as a single-copy reference gene. *P* values were obtained by the two-sided Mann-Whitney *U* test.

AtALKBH9B and m^{6}A-methylated RNAs are localized to SGs under heat

Our results thus far indicated that the *atalkbh9b* mutant exhibits opposing patterns to different *Onsen* intermediates, i.e., increased RNA and reduced DNA levels. We speculated that such divergence might be caused by RNA sequestration that inhibits the conversion of RNA to DNA intermediates. Previous studies in humans demonstrated a strong association of methylated RNAs with SGs (*49*, *50*). An SG is an evolutionarily conserved intracellular compartment that is formed under stress conditions and stores proteins and RNAs (*51*–*54*). We therefore hypothesized that hypermethylated *Onsen* RNA in *atalkbh9b* might be localized in SGs and was precluded from where eclDNA production occurs. To test this hypothesis, we first investigated whether the AtALKBH9B protein was localized in SGs. We expressed AtALKBH9B-GFP in tobacco leaves along with SUPPRESSOR OF GENE SILENCING 3 (SGS3)–TdTomato as an SG marker. As shown in Fig. 4A, cytoplasmic foci of SGs were formed under heat stress, and AtALKBH9B-GFP colocalized with SGS3-TdTomato. The association of AtALKBH9B with SGs was further examined in double transgenic *Arabidopsis* plants expressing both AtALKBH9B-GFP and SGS3-TdTomato. Consistent with Fig. 4A, AtALKBH9B-GFP was in cytoplasmic foci along with SGS3-TdTomato in *Arabidopsis* root epidermal cells (Fig. 4, B and C). We further investigated the interactome of AtALKBH9B by performing immunoprecipitation (IP)/mass spectrometry (MS) experiments using *Arabidopsis* transgenic plants expressing AtALKBH9B-GFP. Our IP/MS data identified many proteins that were previously known as SG components (Fig. 4D, fig. S7, and tables S1 and S2). Notably, the YTH domain-containing m^{6}A reader proteins ECT1 and ECT2 were identified in the AtALKBH9B interactome (Fig. 4D and tables S1 and S2). It is also worth noting that a substantial fraction of AtALKBH9B-interacting proteins is commonly found in the previously reported SG proteome data (table S2) (*55*). Among those proteins that are in both the AtALKBH9B interactome and SG proteome, ECT2 was chosen for further testing of its interaction with AtALKBH9B. We performed split luciferase assay experiments in tobacco leaves and observed a notable protein-protein interaction between AtALKBH9B and ECT2 (Fig. 4E). Two other SG marker proteins, UBP1b and PAB2, were also tested for their interaction with 9B in split luciferase assays, and we were able to detect the interaction between AtALKBH9B and SG marker proteins (fig. S8). Overall, AtALKBH9B is localized to SGs and interacts with multiple SG components.

We next investigated whether m^{6}A-methylated RNAs are preferably localized to SGs in *Arabidopsis*. For this, we carried out RNA dot blot experiments with an m^{6}A antibody using the RNAs extracted from the SG fraction of the heat-stressed *atalkbh9b-1* mutants (fig. S9). Compared to total RNA, SG RNA showed a higher level of m^{6}A RNA modification (Fig. 5, A and B), which is consistent with what is known in mammalian SGs (*49*, *50*). RNA-seq was also performed using the total and SG RNAs derived from the heat-stressed WT and *atalkbh9b-1* mutant. We observed that the SG-enriched RNAs contained a higher number of m^{6}A peaks than total RNAs (Fig. 5C). To directly detect the m^{6}A RNA modification in the SG-enriched transcripts, the ONT-DRS experiment

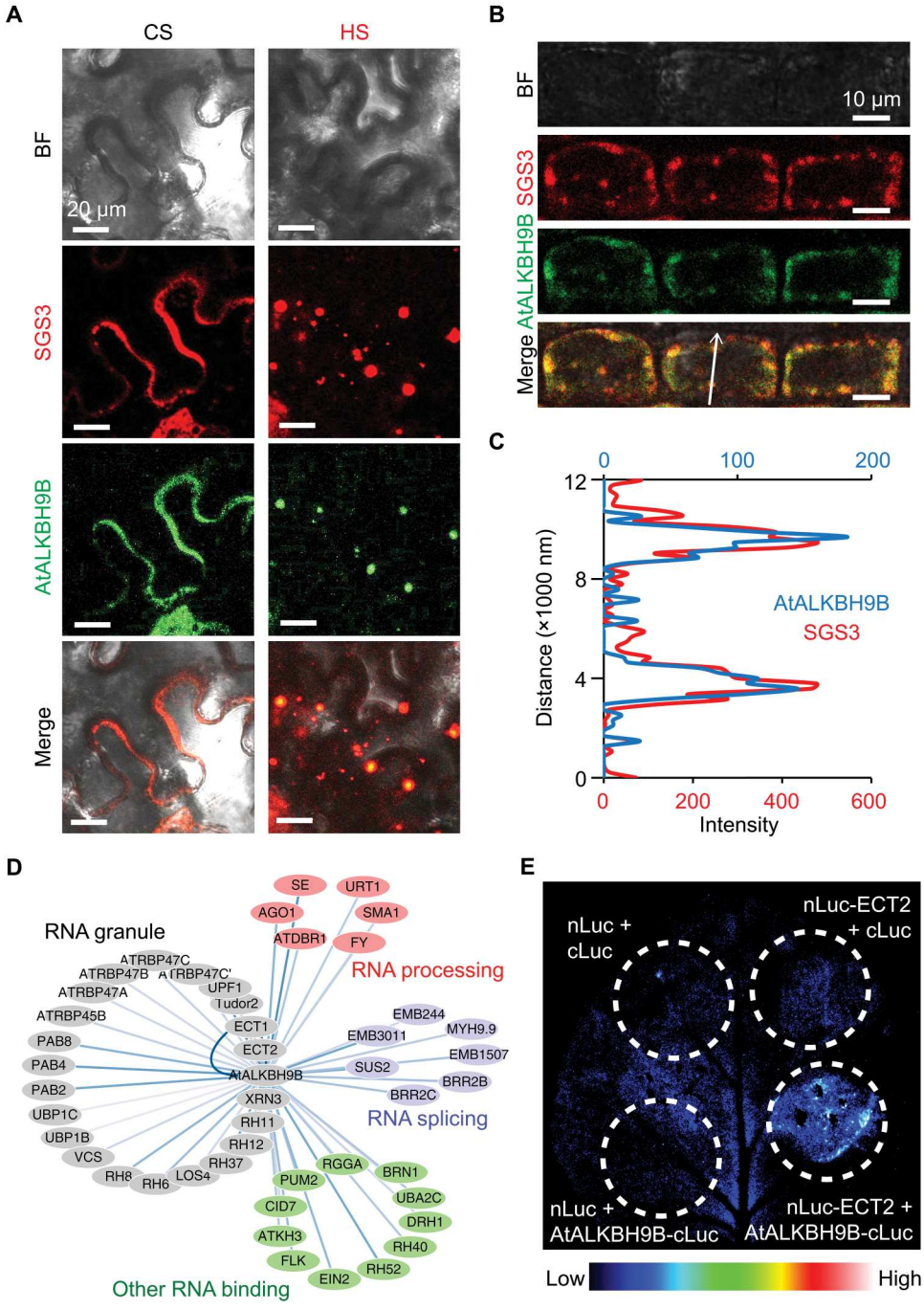

Fig. 4. AtALKBH9B is localized to SGs upon heat. (**A**) Colocalization of AtALKBH9B-GFP and SGS3-TdTomato tested in tobacco transient expression system. HS, heat-stressed for 12 hours. Scale bars, 20 μm. (**B** and **C**) Colocalization of AtALKBH9B-GFP and SGS3-TdTomato in *Arabidopsis* double transgenic plants subjected to heat stress for 12 hours (B). Root epidermal cells of heat-stressed plants are shown. Arrow indicates the section for which the signal intensity was quantitated (C). Scale bars, 10 μm. (**D**) Interactome of AtALKBH9B revealed by IP/MS. Heat-stressed *pUBQ10::AtALKBH9B-GFP* transgenic *Arabidopsis* plants were used. Proteins are color-coded by their functional categories. Edges with darker color represent stronger protein-protein interactions. The IP/MS experiment was performed with three independent biological replicates. Proteins with the $-10\log_{10}P$ values greater than 20 were filtered, and those involved in RNA regulation were chosen for visualization. (**E**) Interaction of AtALKBH9B and ECT2 determined by a split luciferase assay performed in tobacco transient expression system.

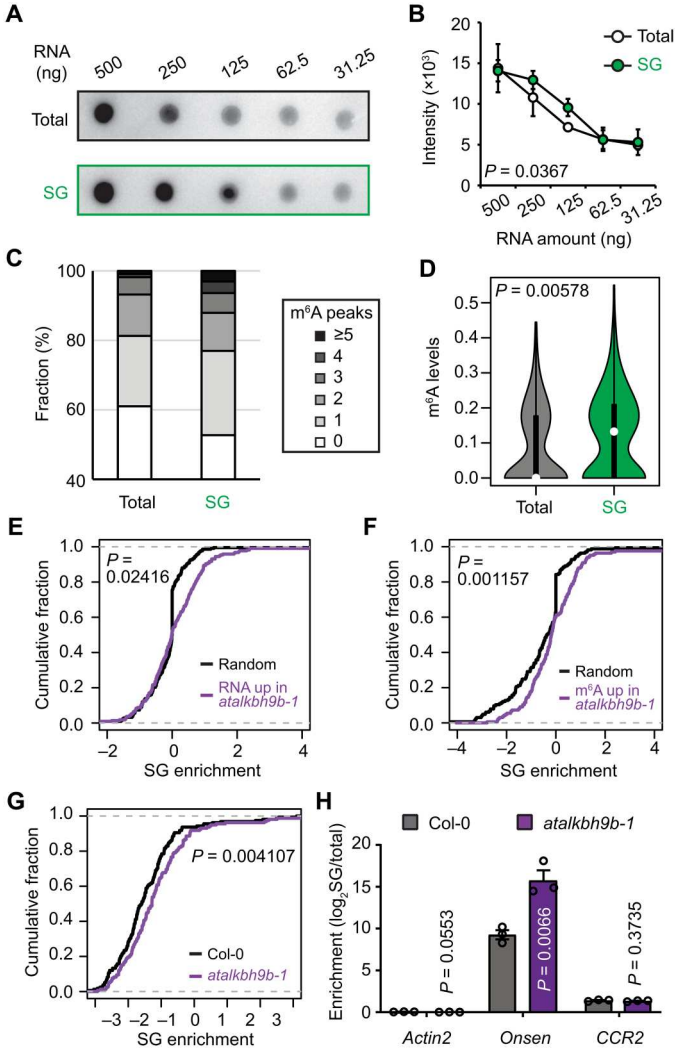

Fig. 5. SG enrichment of m^{6}A-modified RNA. (**A**) RNA dot blot analysis of m^{6}A RNA modification in the total and SG-enriched RNA. Total and SG RNA derived from the 24-hour heat-stressed *atalkbh9b-1* mutant plants were used. (**B**) Signal intensity of the blot shown in (A) is quantitated. Values are means ± SD from three biological replications. (**C**) Number of m^{6}A peaks in the total and SG-enriched transcripts. SG enrichment score is defined as the $\log_2$-transformed fold change of SG to total RNA levels. SG-enriched transcripts are those with SG enrichment score greater than 1. (**D**) m^{6}A levels of the SG-enriched transcripts detected by ONT-DRS. m^{6}A level of a transcript was determined by the mean fraction of m^{6}A RNA modification from all detected m^{6}A sites by ONT-DRS. Transcripts with FPKM values greater than 10 are only considered. SG-enriched transcripts are those with SG enrichment score greater than 0.5 (n = 194). P values were obtained by the one-sided Wilcoxon rank sum text. (**E** to **G**) In (E), cumulative distribution for the SG enrichment of the transcripts up-regulated in *atalkbh9b-1* ($\log_2$-fold change ≥ 1, n = 217) as compared with the randomly selected transcripts (n = 217). In (F), SG enrichment of the transcripts hypermethylated in *atalkbh9b-1* (Δm^{6}A ≥ 0.2, n = 165). In (G), SG enrichment score is compared between WT and *atalkbh9b-1*. P values were obtained by the one-sided Wilcoxon rank sum text. (**H**) SG enrichment of *Onsen* RNA in the *atalkbh9b-1* mutant determined by qPCR. Normalization was against total RNA. *CCR2* was used as a negative control which is strongly marked by m^{6}A but is not regulated by AtALKBH9B (fig. S10). Data are shown in means ± SD from three biological replications. P values were obtained by the two-tailed Student's t test.

was performed. Figure 5D shows that the transcripts that were strongly associated with SG exhibited higher levels of m^{6}A RNA methylation in the SG fraction. We then identified the transcripts up-regulated in *atalkbh9b-1* from the RNA-seq data shown in Fig. 5C and compared their SG enrichment. When compared with randomly selected RNAs, the AtALKBH9B-regulated transcripts showed stronger SG enrichment (Fig. 5E). A similar result of stronger SG enrichment was also observed for the transcripts that were hypermethylated in *atalkbh9b-1* (Fig. 5F). SG enrichment was also compared in the WT and *atalkbh9b* for the hypermethylated transcripts, and we observed a marked increase in SG enrichment in the *atalkbh9b-1* mutant (Fig. 5G). The enhancement of SG localization of *Onsen* RNA in *atalkbh9b-1* was further validated by qPCR using *CCR2* as a negative control (fig. S10). Figure 5H shows that the SG enrichment of *Onsen* RNA was increased in the *atalkbh9b-1* mutant. We also tested the mutants for SG components and observed that the *Onsen* RNA levels were decreased in these mutants (fig. S11), which partly indicates that SG stabilizes *Onsen* RNA. In short, the AtALKBH9B protein and m^{6}A-methylated transcripts are localized in cytoplasmic SGs under heat stress.

m^{6}A inhibits VLP assembly and eclDNA production

We have demonstrated that m^{6}A-methylated *Onsen* RNA is localized in SGs and that AtALKBH9B demethylates it, allowing for its mobilization. It is, however, important to note that neo-insertions of *Onsen* are hardly detectable in the WT background (*12*, *43*). We thus postulated additional inhibitory effects of m^{6}A RNA modification on the retrotransposition of *Onsen* other than RNA sequestration to SGs. Because the production of pre-integrational DNA intermediates occurs in virus-like particles (VLPs) and the physical interaction between template RNA and retroelement-encoded Gag protein is the first step of it (*4*, *42*), we tested whether the methylation status of RNA influences the affinity of Gag with RNA. A fluorescence polarization assay was carried out to determine the in vitro binding activity of Gag using RNA oligonucleotides that are identical in sequence but differ in m^{6}A methylation status. As shown in Fig. 6A, the m^{6}A-modified RNA exhibited an increased dissociation constant (K_d) value compared to the nonmethylated RNA, suggesting that m^{6}A inhibits the binding to Gag. We further examined the interaction of Gag and *Onsen* RNA by performing RIP-qPCR experiments using Gag-GFP–expressing transgenic *Arabidopsis* plants (fig. S12). Gag-GFP showed strong binding enrichment to *Onsen* RNA; however, when Gag-GFP was expressed in the *atalkbh9b-1* mutant background, the binding enrichment was markedly reduced (Fig. 6B). In addition, we speculated that m^{6}A RNA methylation might interfere with the reverse transcription (RT) process. To test this possibility, partial *Onsen* RNA was in vitro transcribed in the presence or absence of m^{6}A substrate and subjected to the RT reaction. Consistent with previous studies suggesting that reverse transcriptional activity can be compromised by RNA modifications (*56*, *57*), the m^{6}A-modified RNA showed higher quantification cycle (C_q) values (fig. S13), which indicates that RNA methylation inhibited cDNA production. Together, these data suggest that m^{6}A RNA methylation contributes to retrotransposition suppression by inhibiting VLP assembly and eclDNA production.

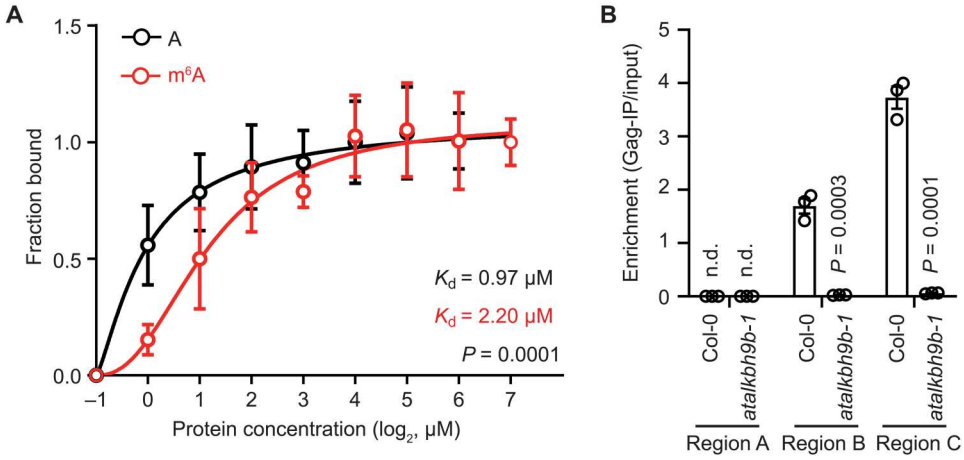

Fig. 6. m^{6}A RNA methylation inhibits binding of Gag in vitro and in vivo. (**A**) Fluorescence polarization assay of purified Gag protein encoded by *Onsen*. RNA oligos (12-mer) with or without m^{6}A modification (GGCCAACUACGU and GGCCAm^{6}ACUACGU) were used. Data are shown in means ± SD from four technical replications. *P* values were obtained by the two-way analysis of variance (ANOVA). (**B**) RIP-qPCR of Gag-GFP binding to *Onsen* transcript. The *OnsenLTR::Gag-GFP* construct was introgressed to *atalkbh9b-1* by genetic cross. Regions tested are as described in Fig. 1E. Data are shown in means ± SD from three biological replications. *P* values were obtained by the two-tailed Student's *t* test. n.d., not determined.

DISCUSSION

In this study, we showed that the heat-activated retrotransposon *Onsen* is m^{6}A-modified and localized to cytoplasmic SGs (Figs. 1 5, and 7). m^{6}A RNA methylation not only leads to spatial constraints preventing RNA maturation to eclDNA but also biochemically inhibits VLP assembly and RT (Figs. 6 and 7 and fig. S13). The SG-localized RNA demethylase AtALKBH9B directly targets *Onsen* RNA and allows it to complete the retrotranspositional process (Figs. 2 and 3). Our study provides insight into the biological role of SGs as sites for the seclusion of transposon RNAs and thus the suppression of their mobility. This notion is partially in agreement with previous work in mammals that suggested the m^{6}A-mediated inhibition of transposons through RNA destabilization, which presumably occurs in cytoplasmic RNA granules (*32*, *33*). However, the discrepancy between the roles of m^{6}A in *Arabidopsis* and those in animals is that it does not trigger strong RNA decay but is associated with RNA stabilization (*24*, *58*). Our data also showed that the depletion of SG components results in the reduction of *Onsen* RNA levels (fig. S11), indicating that SG enhances RNA stability. Together, these results indicate that m^{6}A RNA methylation of *Onsen* guides RNA to SGs without compromising their RNA stability.

m^{6}A RNA methylation presumably occurs cotranscriptionally in the nucleus by RNA methyltransferases that broadly target nascent transcripts with limited specificity (*59*–*61*), and more than 10000 transcripts were found to be methylated in our study (Fig. 1 and fig. S14). Intriguingly, SG localization seems to occur selectively in a subset of m^{6}A-modified transcripts (Fig. 5 and fig. S14), although the responsible m^{6}A reader protein is unknown. A recent study on ECT2, a m^{6}A-binding and SG-localized protein, hints at possible mechanisms for the selective guidance of m^{6}A-modified transcripts to SGs (*62*). The ECT2-binding transcriptome revealed a strong sequence bias toward U that is enriched around m^{6}A-modified sites (*62*). A similar sequence bias of high AU contents in transposon RNA was shown in our previous report (*54*). Therefore, it can be speculated that certain sequence features recognized by m^{6}A reader proteins provide selectivity to m^{6}A-mediated SG localization.

Furthermore, we noticed that AtALKBH9B regulates only a few transcripts in SGs including *Onsen* (fig. S14). AtALKBH9B was previously characterized to localize to SGs and facilitate viral infectivity (*37*), which is similar to what we observed for the *Onsen* retroelement. AtALKBH9B is peculiar and distinct from AtALKBH10B, the other active RNA demethylase in *Arabidopsis*. For example, unlike many other RNA demethylases, AtALKBH9B is localized to cytoplasmic foci and regulates relatively fewer transcripts (*27*, *36*). In addition, we showed that the *Onsen* transcript levels were not altered in the *atalkbh10b* mutants and were controlled specifically by AtALKBH9B (Fig. 2 and fig. S5). These results imply the functional diversification of RNA demethylases and indicate that AtALKBH9B might have evolved to preferentially target nonnative and invasive genetic elements such as retroviruses and retrotransposons. Further investigation of the biochemical characterization of the AtALKBH9B protein will be required to understand target-specific RNA demethylation. In addition, because several m^{6}A reader proteins were identified as AtALKBH9B-interacting partners (Fig. 4), it will also be important to test whether these proteins have a role in the specific RNA target recognition of AtALKBH9B.

In summary, mobile genetic elements are subject to multilayered repression at the transcriptional and posttranscriptional steps. Our work suggests a previously unknown mechanism for the suppression of transposon mobilization that involves m^{6}A RNA methylation and the localization of TE RNA in SGs. The retrotransposon *Onsen* provides an intriguing example of adopting a host factor to bypass such suppression.

MATERIALS AND METHODS

Plant materials and growth condition

Arabidopsis mutants used in this study are in the Col-0 background and were obtained from the Nottingham Arabidopsis Stock Centre

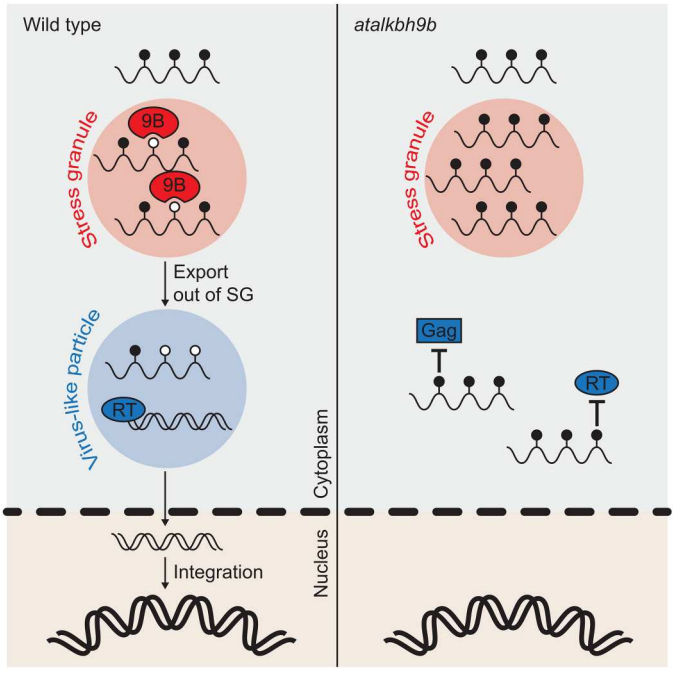

Fig. 7. A proposed model. m^{6}A-modified *Onsen* RNA is localized to SG. AtALKBH9B demethylates and releases *Onsen* RNA out of SG. Demethylated *Onsen* RNA assembles to VLP by interacting with Gag and is reverse-transcribed to form ecIDNA. In the mutant of *AtALKBH9B*, *Onsen* RNA is hypermethylated and localized in SG. In addition, RNA methylation inhibits the binding of Gag and RT. Closed and open circles represent m^{6}A-methylated and unmethylated sites, respectively; dashed line indicates nuclear envelop; wavy single line is RNA, and wavy double line is DNA.

(*atalkbh9b-1*, SALK_015591C; *g3bpl-1*, SALK_011708; *sgs3-14*, SALK_001394; *rdr6-11*, CS24285; *ago7-1*, SALK_037458; and *nrpd1a-3*, SALK_128428). To induce de novo mutations in *AtALKBH9B*, a CRISPR-Cas9 vector was constructed by cloning three single-guide RNAs (sgRNAs) (sequences are provided in table S3) into the Cas9-containing binary vector. The oligonucleotides encoding the sgRNAs were first cloned into the pENTR_L4_R1, pENTR_L1_L2, and pENTR_R2_L3 entry vectors at the Bbs I sites. The entry vectors containing the sgRNAs were then cloned into the destination vector by the attL x attR recombination (LR) reaction using a MultiSite Gateway Pro kit (Thermo Fisher Scientific). The resulting vector was transferred to *Agrobacterium tumefaciens* strain GV3101 and transformed into Col-0 *Arabidopsis* plants. As the vector carries a GFP fluorescence gene driven by a seed coat–specific promoter, the collected T1 seeds were illuminated with the LUYOR-3415RG Dual Fluorescent Protein Flashlight to identify the transformants. T-DNA was segregated out at T2 generation by genotyping the Cas9-encoding gene, and the gene editing events were identified by PCR amplifying the targeted region followed by Sanger sequencing (table S3). For a mutant complementation test of *atalkbh9b-1*, the fluorescence-tagged AtALKBH9B transgenic plants were obtained by constructing a vector *pAtALKBH9B::AtALKBH9B-GFP:tHSP18.2*. Each fragment was PCR-amplified using the primers listed in table S3 and was cloned into the pCAMBIA1300 using the T4 DNA ligase [New England Biolabs (NEB)]. The construct was transformed into the *atalkbh9b-1* mutant, and the transgenic lines were identified for homozygosity at T3 generation.

Arabidopsis seeds were surface sterilized in 75% ethanol for 15 min, washed with 100% ethanol for 1 min, and planted on half-strength Murashige-Skoog medium (including 1% sucrose). Before germination, seeds were stratified for 2 days at 4°C under the dark condition and moved to a growth chamber set at 22°C and 12-hour light/12-hour dark cycle. For the heat stress treatment, plants were grown for 6 days at 22°C and then treated with heat stress of 37°C for 24 hours.

Reverse transcription quantitative polymerase chain reaction

Plant samples were flash-frozen and ground in liquid nitrogen. Total RNA was isolated using the TRIzol Universal Reagent (Tiangen). Briefly, 100 mg of the ground tissue powders were resuspended in 1 ml of TRIzol reagent, incubated at room temperature for 5 min, and then centrifuged at top speed for 10 min at 4°C. The supernatant was mixed vigorously with chloroform and centrifuged at top speed for 10 min at 4°C. The upper phase was mixed with the same volume of isopropanol and incubated at −80°C for 10 min. The RNA was precipitated by centrifugation, and the pellet was washed with 1 ml of 75% ethanol.

The first-strand cDNA synthesis was performed using 500 ng of RNA by the ReverTra Ace qPCR RT Master Mix with gDNA Remover (Toyobo). The resulting cDNA was diluted fourfold with diethyl pyrocarbonate–treated water, and 1.5 μl was used for a 20-μl qPCR reaction mixture. The qPCR was carried out using the ChamQ Universal SYBR qPCR Master Mix (Vazyme) in the CFX96 Connect Real-time PCR Detection system (Bio-Rad). *Actin2* was used as the internal control, and the sequences of the primers used for RT-qPCR are provided in table S3.

RNA immunoprecipitation quantitative polymerase chain reaction

Direct binding of a protein to RNA was assessed by RIP-qPCR experiments. Seven-day-old seedlings heat-stressed at 37°C for 1 day were flash-frozen and ground in liquid nitrogen. Over 2 g of frozen powder was homogenized in 6 ml of extraction buffer [100 mM tris-HCl (pH 7.5), 150 mM NaCl, 0.5% Octylphenoxy poly(ethyleneoxy)ethanol (IGEPAL) (Sigma-Aldrich), and 1% plant protease inhibitor cocktail (MedChemExpress)]. The crude extract was incubated at 4°C for 30 min with shaking and then centrifuged for 30 min at 18,000*g* at 4°C. A ribonuclease (RNase) inhibitor (87.5 μl) (40 U/μl; ABclonal) and GFP-trap magnetic beads (25 μl) (Chromo-Tek) were added to 3.5 ml of the supernatant and incubated overnight at 4°C. The supernatant (350 μl) was kept as an input sample and stored at −80°C freezer until use. After washing four times with 1 ml of extraction buffer, the beads were resuspended in 150 μl of the proteinase K buffer [15 μl of 10% SDS, 18 μl of proteinase K (10 mg/ml), and 117 μl of extraction buffer] and incubated for 30 min at 55°C. RNA was then extracted by adding 400 μl of phenol:chloroform:isopropanol. The mixture was vortexed rigorously for 15 s and centrifuged at 14,000*g* for 10 min at room temperature. The aqueous phase (350 μl) was mixed with 400 μl of chloroform, vortexed, and centrifuged at 14,000*g* for 10 min at room temperature. The aqueous phase (300 μl) was carefully moved to a new tube and added with 30 μl of 3 M sodium acetate (pH 5.2) and 750 μl of 100% ethanol. The mixture was incubated at −80°C overnight and centrifuged at

14,000*g* for 30 min at 4°C. The pellet was washed with 80% ethanol, air-dried, and resuspended in 15 μl of RNase-free water. The input fraction was subjected to the same procedure to extract RNA. The extracted RNAs were reverse-transcribed and analyzed in qPCR as described above in RT-qPCR (the oligonucleotide sequences are provided in table S3). The *OnsenLTR::Gag-GFP* was constructed by modifying the pGPTVII binary vector (*44*) using the primers listed in table S3. The construct was transformed into Col-0 *Arabidopsis* plants and introduced to the *atalkbh9b-1* mutant by genetic cross.

The m^6A enrichment experiment was performed as described previously with minor modifications (*63*) and the Magna RIP RNA-Binding Protein Immunoprecipitation Kit (Merck) was used following the manufacturer′s instruction. Briefly, 300 μg of total RNA was randomly fragmented into 250-nucleotide fragments by RNA fragmentation reagents [for 1 ml of 10× reagents: 800 μl 1 M tris-HCl (pH 7.0), 100 μl of 1 M $ZnCl_2$, and 100 μl of RNase-free H_2O]. Fragmented RNA was precipitated using 2.5 volume of ethanol, 1/10 volume of 3 M NaOH, and glycogen (100 μg/ml) at −80°C overnight. After centrifugation at 14,000*g* for 10 min, the pellet was resuspended in 55 μl of RNase-free H_2O. RNA (5 μl) was kept as the input sample and the remaining RNA was incubated with 5 μg m^6A-specific antibody (cat. no. 202003, Synaptic Systems) overnight at 4°C. The m^6A-containing fragments were pulled down with magnetic beads. The beads were then washed five times using 500 μl of cold RIP Wash Buffer, resuspended in 150 μl of proteinase K buffer [117 μl of RIP Wash Buffer, 15 μl of 10% SDS, and 18 μl of proteinase K (10 mg/ml)], and incubated at 55°C for 30 min with shaking. After incubation, the beads were separated on magnetic rack, and the supernatant was mixed with 250 μl of RIP Wash Buffer. Phenol:chloroform:isoamyl alcohol (400 μl) was added, and the mixture was centrifuged at 14,000g for 10 min at room temperature. The aqueous phase (350 μl) was then mixed with 400 μl of chloroform, and the mixture was centrifuged at 14,000*g* for 10 min at room temperature. The aqueous phase (300 μl) was mixed with 50 μl of Salt Solution I, 15 μl of Salt Solution II, 5 μl of Precipitate Enhancer, and then 850 μl of absolute ethanol. The mixture was stored at −80°C overnight to precipitate the RNA. Then, the mixture was centrifuged at 14,000*g* for 30 min at 4°C, and the pellet was washed with 80% ethanol. After centrifugation at 14,000*g* for 15 min at 4°C, the pellet was resuspended in 20 μl of RNase-free H_2O. The extracted RNAs were reverse-transcribed and analyzed in qPCR as described above in RT-qPCR (the oligonucleotide sequences are provided in table S3).

Amplification of linear extrachromosomal DNA quantitative polymerase chain reaction

ALE-qPCR was performed as previously described (*42*, *64*). Genomic DNA (gDNA) was extracted using the DNeasy Plant Mini Kit (Qiagen) following the manufacturer′s instruction. gDNA (200 ng) and PCR-amplified *Evade* DNA (1 pg) were used for ligation with 0.5 μl of 40 μM adapter DNA overnight at 16°C (the sequences are provided in table S3). The adapter-ligated DNA was purified by AMPure XP beads (Beckman Coulter) at a 1:0.5 ratio. In vitro transcription reactions were performed using the Standard RNA Synthesis Kit (NEB). Purified RNA (1 μg) was subjected to RT using the Transcriptor First Strand cDNA Synthesis Kit (Roche), and 1 μl of RNase A/T1 (Thermo Fisher Scientific) was added to digest nontemplated RNA for 30 min at 37°C. Subsequently, qPCR was performed as described above (the oligonucleotide sequences are provided in table S3).

Induction of *Onsen* retrotransposition

To detect the retrotransposition of *Onsen*, *Arabidopsis* seedlings were grown in the medium containing zebularine (Sigma-Aldrich) and α-amanitin (MCE) and then heat-stressed as described above. The chemical reagents were prepared by filter sterilization (zebularine, 5 mg/ml in dimethyl sulfoxide; and α-amanitin, 1 mg/ml in water) and used at the concentrations indicated in the previous study (*43*). The heat-stressed plants were transferred to soil and grown to maturity under the 16-hour light/8-hour dark cycle at 22°C, and the seeds were harvested from individual plants. DNA was extracted from a whole seedling that was randomly selected and subjected to either ddPCR or whole-genome resequencing. *nrpd1a-3 atalkbh9b-1* double mutant was identified in F2 segregation population derived from a cross of two single mutants. Plants containing the *nrpd1a-3* mutation were grown in the medium without zebularine and α-amanitin.

Droplet digital PCR

The ddPCR experiments were carried out as previously described with minor modifications (*48*). gDNA was extracted using the N96 DNAsecure Plant Kit (Tiangen) following the manufacturer′s instruction. gDNA (100 ng) was digested using AluI for 4 hours at 37°C. The digested DNA was diluted to 0.15 ng/μl using the Qubit4 DNA quantification system (Thermo Fisher Scientific), and the Probe ddPCR SuperMix mixture was prepared (Targeting One; 15 μl of 2× SuperMix, 2.4 μl (10 μM) for each primer, 0.75 μl of fluorescein amidites (FAM) probe (10 μM), 0.75 μl of hexachlorofluorescein (HEX) probe (10 μM), and 3.9 μl of diluted DNA totaling 30 μl). Droplets were generated using the Drop maker (Targeting One), and PCR was performed as following: 95°C for 10 min; then 55 cycles of 94°C for 30 s and 56.8°C for 30 s; and 98°C for 10 min. PCR products were read by a Chip reader system (Targeting One). *CBF2* was used as the internal single-copy control. The oligonucleotide sequences are provided in table S3.

SG enrichment

Enrichment of cytoplasmic RNA granules was performed following the previously described method (*54*, *65*). Briefly, 2 g of seedlings was ground in liquid nitrogen and resuspended in 5 ml of lysis buffer [50 mM tris-HCl (pH 7.4), 100 mM KOAc, 2 mM MgOAc, 0.5 mM dithiothreitol, 0.5% NP-40, cOmplete EDTA-free protease inhibitor cocktail (Roche), and RNasin Plus RNase inhibitor (40 U/ml; Promega)]. The mixture was filtered through four layers of Miracloth (Sigma-Aldrich) and centrifuged at 4000*g* for 10 min at 4°C. The supernatant was removed, and the pellet was resuspended in 2 ml of lysis buffer. The samples were again centrifuged at 18,000*g* for 10 min at 4°C. The pellet was resuspended in 2 ml of lysis buffer, vortexed, and centrifuged at 18,000*g* at 4°C for 10 min. The supernatant was discarded, and the pellet was resuspended in 1 ml of lysis buffer. After a brief centrifugation at 850*g* for 10 min at 4°C, the RNA granule fraction in the supernatant was collected for RNA extraction. To verify the SG enrichment, we generated the transgenic *pUBQ10::mCherry-UBP1B Arabidopsis* plants. Briefly, the gDNA of *UBP1B* was cloned into pCAMBIA1300 that contains N-terminal mCherry tag and introduced to Col-0 (sequences of primers used for cloning are provided in table S3). Validation of the enrichment

of SGs was performed by Western blots using the anti-Actin (1:1000; 26F7, Abmart) and anti-SGS3 [1:1000; (*66*)] antibodies.

RNA dot blot

The extracted total and SG RNA was serially diluted and spotted on polyvinylidene difluoride membrane (Bio-Rad). The membrane was soaked in 1-ethyl-3-(3-dimethylaminopropyl)carbodiimide (EDC; Thermo Fisher Scientific) solution [125 mM 1-methyl imidazole (pH 8) and EDC (31.375 mg/ml)] and incubated at 65°C for 2 hours for cross-linking. The cross-linked membrane was washed four times with TBST buffer [150 mM NaCl, 20 mM tris-HCl (pH 8.0), and 0.05% Tween 20]. After blocking with 5% skim milk, the membrane was incubated in TBST buffer containing anti-m^{6}A antibody (Synaptic Systems) overnight at 4°C with gentle agitation. Subsequently, the membrane was washed with TBST buffer four times and incubated in TBST buffer containing horseradish peroxidase–conjugated anti-rabbit immunoglobulin G (Abmart) at room temperature for 1 hour. The secondary antibody was poured out, added with TBST, and washed four times (5 min each time). Chemiluminescence of the blot was detected using an Omni-ECLTM Femto Light Chemiluminescence kit (EpiZyme), and images were acquired by Tanon-5200 (Tanon).

Next-generation sequencing

mRNA was purified from 3 μg of total RNA using the poly(T) oligo-attached magnetic beads (Thermo Fisher Scientific). Library preparation was performed using the NEBNext Ultra RNA Library Prep Kit (NEB) following the manufacturer's instructions. Sequencing was performed on an Illumina NovaSeq 6000 platform, and 150–base pair paired-end reads were generated.

For the data analysis, the raw sequences were processed using Trimmomatic (version 0.39) (*67*) to remove the adapter and low-quality sequences. Trimmed reads were then aligned to the *Arabidopsis* reference genome (TAIR10) with default settings using Hisat2 (version 2.2.1) (*68*). The fragments per kilobase of transcript per million mapped reads (FPKM) values of genes and TEs were calculated by StringTie (version 2.1.7) (*69*). TEs that are annotated as genes in TAIR10 annotation were used in our analysis. Visualization of the sequencing data was performed using the Integrative Genomics Viewer (*70*). For the m^{6}A peak calling, model-based analysis of ChIP-seq 2 (MACS2) (version 2.2.7.1) (*71*) was run with the following parameters; --nomodel,--extsize 50, -p 5e-2, and -g 65084214 (the -g option accounts for the size of the *Arabidopsis* transcriptome). The m^{6}A peaks detected in both biological replications were chosen and used in the subsequent analyses. Next-generation sequencing (NGS) data generated in this study are summarized in table S4.

Oxford Nanopore Technologies direct RNA-seq

Total RNA was isolated by TRIzol (Qiagen), and poly(A) RNA was purified using the Dynabeads mRNA Purification Kit (Invitrogen) following the manufacturer's instructions. The quality and quantity of poly(A) mRNA were assessed using both the NanoDrop 2000 spectrophotometer and Qubit. The library was prepared using a direct RNA-seq kit (Nanopore, SQK-RNA002), loaded onto an R9.4 Flow Cell (Flow cell type FLO-MIN106), and sequenced on a GridION device for 48 hours.

The raw nanopore signals were converted to base sequences by Guppy (version 4.2.3) using high-accuracy base calling model. The reads with a mean quality score greater than 7 were aligned to the *Arabidopsis* transcriptome (TAIR10 cDNA FASTA) using Minimap2 (version 2.24-r1122) (*72*) with the following parameters: -ax map-ont -p 0 -N 10. NanoCount (version 1.0.0.post6) (*73*) was used to get transcripts per kilobase million (TPM) value, and --max_dist_3_prime was set to −1. Deeplearning explore nanopore m^{6}A (DENA) was adopted to identify m^{6}A sites. Sites supported by at least 10 reads and modification rate more than 0.1 were kept as m^{6}A sites. The coordinates of m^{6}A sites on transcriptome were converted to genome coordinate by "mapFromTranscripts" from GenomicFeatures package. The distribution of m^{6}A on transcripts was checked by Guitar package (*74*). For each transcript, m^{6}A level was defined as an average m^{6}A ratio from all modified sites.

Confocal microscopy

To determine the subcellular localization of SGS3 and AtALKBH9B proteins, the pGPTVII binary vector was modified to generate *pUBQ10::SGS3-TdTomato* and *pUBQ10::AtALKBH9B-GFP* constructs. The coding sequence (CDS) of AtALKBH9B and SGS3 was amplified from Col-0 cDNA using KOD-Plus-Neo (Toyobo) (primers are listed in table S3). The vectors were transformed into Col-0 *Arabidopsis* plants, which were selected on half-strength MS plates containing Glufosinate ammonium (10 μg/ml; Coolaber) and further confirmed by PCR using the primers targeting GFP and TdTomato (listed in table S3). The *AtALKBH9B-GFP SGS3-TdTomato* double transgenic plant was generated from genetic crossing and identified by PCR-based genotyping in F2 populations. The transgenic plants were heat-stressed at 37°C for 12 hours, and the fluorescence signals were detected by Zeiss LSM880 confocal microscopy. For the tobacco transient expression experiments, the constructs were expressed along with P19 in tobacco leaves. Tobacco plants were heat-stressed at 37°C for 12 hours at 48 hours after agro-infiltration.

Immunoprecipitation/mass spectrometry

The 7-day-old seedlings of *pUBQ10::AtALKBH9B-GFP* and *p35S::GFP* were treated with 1-day heat stress under 37°C and immediately flash-frozen. Ground powder (1 g) was homogenized in 3 ml of IP buffer [20 mM Hepes (pH 7.4), 2 mM EDTA, 25 mM NaF, 1 mM Na_3VO_4, 10% glycerol, 100 mM NaCl, 0.5% Triton X-100, and 1% plant protease inhibitor cocktail (MedChemExpress)], and the mixture was rotated at 4°C for 1 hour. The crude extract was centrifuged for 20 min at 18,000*g* at 4°C. The IP was performed using 3 ml of plant extract mixed with 25 μl of GFP-trap magnetic beads (ChromoTek) at 4°C overnight. The beads were washed four times with 1 ml of IP buffer and centrifuged for 1 min at 200*g* at 4°C.

For protein digestion, 100 μg of protein was reduced with 2 μl of 0.5 M tris(2-carboxyethyl)phosphine at 37°C for 60 min and alkylated with 4 μl of 1 M iodoacetamide at room temperature for 40 min in darkness. Fivefold volumes of cold acetone were added to precipitate protein at −20°C overnight. After centrifugation at 12,000*g* at 4°C for 20 min, the pellet was washed twice using 1 ml of prechilled 90% acetone aqueous solution. Then, the pellet was resuspended with 100 μl of 10 mM triethylammonium bicarbonate buffer. Trypsin (Promega) was added at 1:50 trypsin–to–protein mass ratio and incubated at 37°C overnight. The peptide mixture was desalted by C18 ZipTip and lyophilized by SpeedVac.

For nano–high-performance liquid chromatography–tandem MS (MS/MS) analysis, the peptides were analyzed by online nano flow liquid chromatography MS/MS performed on an EASY-nanoLC 1200 system (Thermo Fisher Scientific) connected to a Q Exactive Plus mass spectrometer (Thermo Fisher Scientific). Acclaim PepMap C18 (75 μm by 25 cm) was equilibrated with solvent A (A, 0.1% formic acid in water) and solvent B [B, 0.1% formic acid in acetonitrile (ACN)]. Peptide (3 μl) was loaded and separated with 60-min gradient at flow rate of 300 nl/min. The column temperature was 40°C. The electrospray voltage of 2 kV versus the inlet of the mass spectrometer was used. The peptides were eluted using the following gradient: 0 to 3 min, 2 to 6% B; 3 to 42 min, 6 to 20% B; 42 to 47 min, 20 to 35% B; 47 to 48 min, 35 to 100% B; and 48 to 60 min, maintained 100% B.

The mass spectrometer was run under data-dependent acquisition modeand automatically switched between MS and MS/MS mode. The survey of full-scan MS spectra [mass/charge ratio (m/z), 200 to 1800] was acquired in the Orbitrap with resolution of 70,000. The automatic gain control (AGC) targets at 3×10^6, and the maximum injection time was 50 ms. Then, the top 20 most intense precursor ions were selected into collision cell for fragmentation by higher-energy collision dissociation with the collection energy of 28. The MS/MS resolution was set at 17,500, the AGC targets at 1×10^5, the maximum injection time was 45 ms, isolation window was 2 m/z, and dynamic exclusion was 30 s.

Tandem mass spectra were processed by PEAKS Studio (version 10.6, Bioinformatics Solutions Inc.). PEAKS DB was set up to search the uniprot_Arabidopsis_thaliana (version 201907, entries 27477) database assuming trypsin as the digestion enzyme. PEAKS DB was searched with a fragment ion mass tolerance of 0.02 Da and a parent ion tolerance of 7 parts per million. Carbamidomethylation (C) was specified as the fixed modification. Oxidation (M), deamidation (NQ), and acetylation (K) were specified as variable modifications. The peptides with $-10\log_{10}P \geq 20$ and the proteins with $-10\log P \geq 20$ containing at least one unique peptide were filtered.

Split luciferase complementation assay

The CDS of *AtALKBH9B*, *ECT2*, *UBP1B*, and *PAB2* were amplified by PCR and cloned into the modified pCAMBIA_nLUC and pCAMBIA_cLUC vectors containing the 35*S* promoter (primers are listed in table S3). The constructs were transformed into the *A. tumefaciens* strain GV3101 and then infiltrated into *Nicotiana benthamiana* leaves along with P19. The detached leaves were sprayed with 1 mM luciferin (GLPBio) at 2 days after infiltration. The luminescence signal was visualized with a Tanon-5200 (Tanon).

Fluorescence polarization

The Gag region of *Onsen* was PCR-amplified using the primers listed in table S3, cloned into pET28a-generating 6xHis-Gag, and transformed into *Escherichia coli* strain Rosetta. Starter culture was grown overnight in 4 ml of LB medium containing kanamycin (50 μg/ml) and chloramphenicol (25 μg/ml) at 37°C with shaking at 200 rpm. Starter culture (3 ml) was transferred to 300 ml of LB medium. Cells were grown at 37°C with shaking at 200 rpm until the optical density at 600 nm reach between 0.6 and 0.8. The growth temperature was then lowered to 12°C, and isopropyl-β-D-thiogalactopyranoside was added to a final concentration of 0.5 mM. Cells were incubated for 2 days at 12°C with shaking at 180 rpm and harvested by centrifugation. The pellet was resuspended in 30 ml of lysis buffer [20 mM tris-HCl (pH 7.6), 200 mM NaCl, 10% glycerol, and 0.1% Tween 20]. Sixty microliters of deoxyribonuclease (DNase) I (1 U/μl), 60 μl of 1 M $MgSO_4$, and 150 μl of 200 mM phenylmethylsulfonyl fluoride were added, and the cells were lysed using an SCIENTZ-IID cell homogenizer (SCIENTZ). Lysates were cleared with cell debris by centrifugation at 18,000*g* for 1 hour at 4°C. Cleared lysates were loaded onto an Econo-Pac Chromatography Columns column (Bio-Rad) and washed with 2 column volumes of buffer [20 mM tris-HCl (pH 7.6), 200 mM NaCl, 10% glycerol, 0.1% Tween 20, and 25 mM imidazole]. Bound protein was eluted in 2 ml of buffer [20 mM tris-HCl (pH 7.6), 200 mM NaCl, 10% glycerol, 0.1% Tween 20, and 500 mM imidazole]. Protein was concentrated using a spin concentrator [Amicon, 10K molecular weight cutoff (MWCO)] and injected onto Superdex 200 column (GE Healthcare) equilibrated in 25 mM Hepes (pH 7.5) and 100 mM NaCl. Fractions were checked for purity by SDS–polyacrylamide gel electrophoresis followed by Coomassie blue staining. Fluorescence polarization assay was carried out following the previously described method (*75*). Binding assays were performed in 25 mM Hepes (pH 7.5) and 100 mM NaCl including 10 nM FAM-labeled RNA oligonucleotide (GGCCAACUACGU and GGCCAm^{6}ACUACGU) in black and flat-bottom 96-well plates [British Biocell International (BBI)]. Proteins were serially diluted twofold and the final assay volume was 25 μl per well. The signal was detected at room temperature on a BioTek Synergy Neo plate reader (BioTek). Polarization (P) was converted to anisotropy (A) using the formula $A = 2P/(3 - P)$. Data were plotted as fraction bound by setting the highest anisotropy measured to 1. Data were plotted using GraphPad Prism (version 6.0), and K_d values were obtained by fitting the curve to a nonlinear regression model.

RT efficiency

RT efficiency assay was performed using the MEGAscript RNAi Kit (Thermo Fisher Scientific) according to the manufacturer′s instructions. In brief, the template DNA was amplified using the primers containing T7 promoter (listed in table S3). The in vitro transcription was carried out as follows: 3 μl of 10× T7 Reaction Buffer, 0.5 μl of adenosine 5′-triphosphate (ATP) solution or 0.5 μl of m^{6}ATP (TriLink), 1 μl each of C/G/UTP, 1 μl of T7 RNA polymerase, and 2.5 μl of DNA (500 ng) at 37°C overnight. The template DNA was removed by adding the DNase I and incubating the mixture at 37°C for 2 hours. RNA was purified by the ethanol precipitation method and resuspended in 20 μl of RNase-free H_2O. RNA was reverse-transcribed using the ReverTra Ace qPCR RT Master Mix with gDNA Remover (Toyobo) for 30 s. Subsequently, qPCR was performed as described above. The oligonucleotide sequences are provided in table S3.

Supplementary Materials

This PDF file includes:

Figs. S1 to S14
Tables S1 to S4
Legend for Data S1

Other Supplementary Material for this manuscript includes the following:

Data S1

REFERENCES AND NOTES

1. D. Lisch, How important are transposons for plant evolution? *Nat. Rev. Genet.* **14**, 49–61 (2013).
2. C. Feschotte, Transposable elements and the evolution of regulatory networks. *Nat. Rev. Genet.* **9**, 397–405 (2008).
3. R. Rebollo, M. T. Romanish, D. L. Mager, Transposable elements: An abundant and natural source of regulatory sequences for host genes. *Annu. Rev. Genet.* **46**, 21–42 (2012).
4. V. Satheesh, W. Fan, J. Chu, J. Cho, Recent advancement of NGS technologies to detect active transposable elements in plants. *Genes Genomics* **43**, 289–294 (2021).
5. D. Lisch, Epigenetic regulation of transposable elements in plants. *Annu. Rev. Plant Biol.* **60**, 43–66 (2009).
6. H. Zhang, Z. Lang, J. K. Zhu, Dynamics and function of DNA methylation in plants. *Nat. Rev. Mol. Cell Biol.* **19**, 489–506 (2018).
7. M. A. Matzke, R. A. Mosher, RNA-directed DNA methylation: An epigenetic pathway of increasing complexity. *Nat. Rev. Genet.* **15**, 394–408 (2014).
8. R. K. Slotkin, R. Martienssen, Transposable elements and the epigenetic regulation of the genome. *Nat. Rev. Genet.* **8**, 272–285 (2007).
9. J. A. Law, S. E. Jacobsen, Establishing, maintaining and modifying DNA methylation patterns in plants and animals. *Nat. Rev. Genet.* **11**, 204–220 (2010).
10. A. Madlung, L. Comai, The effect of stress on genome regulation and structure. *Ann. Bot.* **94**, 481–495 (2004).
11. P. Negi, A. N. Rai, P. Suprasanna, Moving through the stressed genome: Emerging regulatory roles for transposons in plant stress response. *Front. Plant Sci.* **7**, (2016).
12. H. Ito, H. Gaubert, E. Bucher, M. Mirouze, I. Vaillant, J. Paszkowski, An siRNA pathway prevents transgenerational retrotransposition in plants subjected to stress. *Nature* **472**, 115–119 (2011).
13. V. V. Cavrak, N. Lettner, S. Jamge, A. Kosarewicz, L. M. Bayer, O. Mittelsten Scheid, How a retrotransposon exploits the Plant's heat stress response for its activation. *PLOS Genet.* **10**, e1004115 (2014).
14. W. Matsunaga, A. Kobayashi, A. Kato, H. Ito, The effects of heat induction and the siRNA biogenesis pathway on the transgenerational transposition of ONSEN, a copia-like retrotransposon in Arabidopsis thaliana. *Plant Cell Physiol.* **53**, 824–833 (2012).
15. W. Matsunaga, N. Ohama, N. Tanabe, Y. Masuta, S. Masuda, N. Mitani, K. Yamaguchi-Shinozaki, J. F. Ma, A. Kato, H. Ito, A small RNA mediated regulation of a stress-activated retrotransposon and the tissue specific transposition during the reproductive period in Arabidopsis. *Front. Plant Sci.* **6**, 1–12 (2015).
16. K. Nozawa, J. Chen, J. Jiang, S. M. Leichter, M. Yamada, T. Suzuki, F. Liu, H. Ito, X. Zhong, DNA methyltransferase CHROMOMETHYLASE3 prevents ONSEN transposon silencing under heat stress. *PLOS Genet.* **17**, e1009710 (2021).
17. S. Liu, J. Jonge, M. S. Trejo-Arellano, J. Santos-González, C. Köhler, L. Hennig, Role of H1 and DNA methylation in selective regulation of transposable elements during heat stress. *New Phytol.* **229**, 2238–2250 (2021).
18. K. D. Meyer, S. R. Jaffrey, Rethinking m6A readers, writers, and erasers. *Annu. Rev. Cell Dev. Biol.* **33**, 319–342 (2017).
19. T. Pan, N6-methyl-adenosine modification in messenger and long non-coding RNA. *Trends Biochem. Sci.* **38**, 204–209 (2013).
20. I. A. Roundtree, M. E. Evans, T. Pan, C. He, Dynamic RNA modifications in gene expression regulation. *Cell* **169**, 1187–1200 (2017).
21. H. Yue, X. Nie, Z. Yan, S. Weining, N6-methyladenosine regulatory machinery in plants: Composition, function and evolution. *Plant Biotechnol. J.* **17**, 1194–1208 (2019).
22. Y. Fu, D. Dominissini, G. Rechavi, C. He, Gene expression regulation mediated through reversible m6A RNA methylation. *Nat. Rev. Genet.* **15**, 293–306 (2014).
23. Y. Yue, J. Liu, C. He, RNA N6-methyladenosine methylation in post-transcriptional gene expression regulation. *Genes Dev.* **29**, 1343–1355 (2015).
24. G. Z. Luo, A. Macqueen, G. Zheng, H. Duan, L. C. Dore, Z. Lu, J. Liu, K. Chen, G. Jia, J. Bergelson, C. He, Unique features of the m6A methylome in Arabidopsis thaliana. *Nat. Commun.* **5**, 5630 (2014).
25. L. Shen, Z. Liang, X. Gu, Y. Chen, Z. W. N. Teo, X. Hou, W. M. Cai, P. C. Dedon, L. Liu, H. Yu, N6-methyladenosine RNA modification regulates shoot stem cell fate in arabidopsis. *Dev. Cell* **38**, 186–200 (2016).
26. J. Scutenaire, J. M. Deragon, V. Jean, M. Benhamed, C. Raynaud, J. J. Favory, R. Merret, C. Bousquet-Antonelli, The YTH domain protein ECT2 is an m^{6}A reader required for normal trichome branching in arabidopsis. *Plant Cell* **30**, 986–1005 (2018).
27. H.-C. Duan, L.-H. Wei, C. Zhang, Y. Wang, L. Chen, Z. Lu, P. R. Chen, C. He, G. Jia, ALKBH10B is an RNA N^6-methyladenosine demethylase affecting arabidopsis floral transition. *Plant Cell* **29**, 2995–3011 (2017).
28. L. Arribas-Hernández, S. Bressendorff, M. H. Hansen, C. Poulsen, S. Erdmann, P. Brodersen, An m^{6}A-YTH module controls developmental timing and morphogenesis in arabidopsis. *Plant Cell* **30**, 952–967 (2018).
29. S. Zhong, H. Li, Z. Bodi, J. Button, L. Vespa, M. Herzog, R. G. Fray, MTA is an Arabidopsis messenger RNA adenosine methylase and interacts with a homolog of a sex-specific splicing factor. *Plant Cell* **20**, 1278–1288 (2008).
30. Y. Shoaib, J. Hu, S. Manduzio, H. Kang, Alpha-ketoglutarate-dependent dioxygenase homolog 10B, an N^6-methyladenosine mRNA demethylase, plays a role in salt stress and abscisic acid responses in Arabidopsis thaliana. *Physiol. Plant.* **173**, 1078–1089 (2021).
31. J. Tang, J. Yang, H. Duan, G. Jia, ALKBH10B, an mRNA m^{6}A demethylase, modulates ABA response during seed germination in arabidopsis. *Front. Plant Sci.* **12**, 712713 (2021).
32. T. Chelmicki, E. Roger, A. Teissandier, M. Dura, L. Bonneville, S. Rucli, F. Dossin, C. Fouassier, S. Lameiras, D. Bourc'his, m^{6}A RNA methylation regulates the fate of endogenous retroviruses. *Nature* **591**, 312–316 (2021).
33. J. Liu, M. Gao, J. He, K. Wu, S. Lin, L. Jin, Y. Chen, H. Liu, J. Shi, X. Wang, L. Chang, Y. Lin, Y.-L. Zhao, X. Zhang, M. Zhang, G.-Z. Luo, G. Wu, D. Pei, J. Wang, X. Bao, J. Chen, The RNA m^{6}A reader YTHDC1 silences retrotransposons and guards ES cell identity. *Nature* **591**, 322–326 (2021).
34. S.-Y. Hwang, H. Jung, S. Mun, S. Lee, K. Park, S. C. Baek, H. C. Moon, H. Kim, B. Kim, Y. Choi, Y.-H. Go, W. Tang, J. Choi, J. K. Choi, H.-J. Cha, H. Y. Park, P. Liang, V. N. Kim, K. Han, K. Ahn, L1 retrotransposons exploit RNA m^{6}A modification as an evolutionary driving force. *Nat. Commun.* **12**, 880 (2021).
35. F. Xiong, R. Wang, J.-H. Lee, S. Li, S.-F. Chen, Z. Liao, L. Al Hasani, P. T. Nguyen, X. Zhu, J. Krakowiak, D.-F. Lee, L. Han, K.-L. Tsai, Y. Liu, W. Li, RNA m6A modification orchestrates a LINE-1–host interaction that facilitates retrotransposition and contributes to long gene vulnerability. *Cell Res.* **31**, 861–885 (2021).
36. D. Mielecki, D. Ł. Zugaj, A. Muszewska, J. Piwowarski, A. Chojnacka, M. Mielecki, J. Nieminuszczy, M. Grynberg, E. Grzesiuk, Novel AlkB dioxygenases—Alternative models for in silico and in vivo studies. *PLOS ONE* **7**, e30588 (2012).
37. M. Martínez-Pérez, F. Aparicio, M. P. López-Gresa, J. M. Bellés, J. A. Sánchez-Navarro, V. Pallás, Arabidopsis m^{6}A demethylase activity modulates viral infection of a plant virus and the m6A abundance in its genomic RNAs. *Proc. Natl. Acad. Sci. U.S.A.* **114**, 10755–10760 (2017).
38. L. Wang, H. Zhuang, W. Fan, X. Zhang, H. Dong, H. Yang, J. Cho, m6A RNA methylation impairs gene expression variability and reproductive thermotolerance in Arabidopsis. *Genome Biol.* **23**, 244 (2022).
39. M. Martínez-Pérez, C. Gómez-Mena, L. Alvarado-Marchena, R. Nadi, J. L. Micol, V. Pallas, F. Aparicio, The m^{6}A RNA demethylase ALKBH9B plays a critical role for vascular movement of alfalfa mosaic virus in arabidopsis. *Front. Microbiol.* **12**, 745576 (2021).
40. L. Alvarado-Marchena, J. Marquez-Molins, M. Martinez-Perez, F. Aparicio, V. Pallás, Mapping of functional subdomains in the atALKBH9B m^{6}A-demethylase required for its binding to the viral RNA and to the coat protein of alfalfa mosaic virus. *Front. Plant Sci.* **12**, 701683 (2021).
41. D. H. Sanchez, J. Paszkowski, Heat-induced release of epigenetic silencing reveals the concealed role of an imprinted plant gene. *PLOS Genet.* **10**, e1004806 (2014).
42. J. Cho, M. Benoit, M. Catoni, H.-G. Drost, A. Brestovitsky, M. Oosterbeek, J. Paszkowski, Sensitive detection of pre-integration intermediates of long terminal repeat retrotransposons in crop plants. *Nat. Plants.* **5**, 26–33 (2019).
43. M. Thieme, S. Lanciano, S. Balzergue, N. Daccord, M. Mirouze, E. Bucher, Inhibition of RNA polymerase II allows controlled mobilisation of retrotransposons for plant breeding. *Genome Biol.* **18**, 1–10 (2017).
44. H. Gaubert, D. H. Sanchez, H. G. Drost, J. Paszkowski, Developmental restriction of retrotransposition activated in Arabidopsis by environmental stress. *Genetics* **207**, 813–821 (2017).
45. Z. Wang, K. Tang, D. Zhang, Y. Wan, Y. Wen, Q. Lu, L. Wang, High-throughput m^{6}A-seq reveals RNA m^{6}A methylation patterns in the chloroplast and mitochondria transcriptomes of Arabidopsis thaliana. *PLOS ONE* **12**, e0185612 (2017).
46. P. Jenjaroenpun, T. Wongsurawat, T. D. Wadley, T. M. Wassenaar, J. Liu, Q. Dai, V. Wanchai, N. S. Akel, A. Jamshidi-Parsian, A. T. Franco, G. Boysen, M. L. Jennings, D. W. Ussery, C. He, I. Nookaew, Decoding the epitranscriptional landscape from native RNA sequences. *Nucleic Acids Res.* **49**, e7 (2021).
47. H. Liu, O. Begik, M. C. Lucas, J. M. Ramirez, C. E. Mason, D. Wiener, S. Schwartz, J. S. Mattick, M. A. Smith, E. M. Novoa, Accurate detection of m^{6}A RNA modifications in native RNA sequences. *Nat. Commun.* **10**, 4079 (2019).
48. W. Fan, J. Cho, Quantitative measurement of transposon copy number using the droplet digital PCR. *Methods Mol. Biol.*, 171–176 (2021).
49. R. J. Ries, S. Zaccara, P. Klein, A. Olarerin-George, S. Namkoong, B. F. Pickering, D. P. Patil, H. Kwak, J. H. Lee, S. R. Jaffrey, m^{6}A enhances the phase separation potential of mRNA. *Nature* **571**, 424–428 (2019).

50. Y. Fu, X. Zhuang, m^{6}A-binding YTHDF proteins promote stress granule formation. *Nat. Chem. Biol.* **16**, 955–963 (2020).
51. J. R. Wheeler, S. F. Mitchell, A. Khong, T. Matheny, R. Parker, S. Jain, The stress granule transcriptome reveals principles of mRNA accumulation in stress granules. *Mol. Cell* **68**, 808–820.e5 (2017).
52. J. A. Riback, C. D. Katanski, J. L. Kear-Scott, E. V. Pilipenko, A. E. Rojek, T. R. Sosnick, D. A. Drummond, Stress-triggered phase separation is an adaptive, evolutionarily tuned response. *Cell* **168**, 1028–1040.e19 (2017).
53. T. Chantarachot, J. Bailey-Serres, Polysomes, stress granules, and processing bodies: A dynamic triumvirate controlling cytoplasmic mrna fate and function. *Plant Physiol.* **176**, 254–269 (2018).
54. E. Y. Kim, L. Wang, Z. Lei, H. Li, W. Fan, J. Cho, Ribosome stalling and SGS3 phase separation prime the epigenetic silencing of transposons. *Nat. Plants* **7**, 303–309 (2021).
55. M. Kosmacz, M. Gorka, S. Schmidt, M. Luzarowski, J. C. Moreno, J. Szlachetko, E. Leniak, E. M. Sokolowska, K. Sofroni, A. Schnittger, A. Skirycz, Protein and metabolite composition of Arabidopsis stress granules. *New Phytol.* **222**, 1420–1433 (2019).
56. P. Ryvkin, Y. Y. Leung, I. M. Silverman, M. Childress, O. Valladares, I. Dragomir, B. D. Gregory, L.-S. Wang, HAMR: High-throughput annotation of modified ribonucleotides. *RNA* **19**, 1684–1692 (2013).
57. S. A. Woodson, J. G. Muller, C. J. Burrows, S. E. Rokita, A primer extension assay for modification of guanine by Ni(II) complexes. *Nucleic Acids Res.* **21**, 5524–5525 (1993).
58. S. J. Anderson, M. C. Kramer, S. J. Gosai, X. Yu, L. E. Vandivier, A. D. L. Nelson, Z. D. Anderson, M. A. Beilstein, R. G. Fray, E. Lyons, B. D. Gregory, N^6-methyladenosine inhibits local ribonucleolytic cleavage to stabilize mRNAs in Arabidopsis. *Cell Rep.* **25**, 1146–1157.e3 (2018).
59. B. Slobodin, R. Han, V. Calderone, J. A. F. O. Vrielink, F. Loayza-Puch, R. Elkon, R. Agami, Transcription impacts the efficiency of mRNA translation via co-transcriptional N^6-adenosine Methylation. *Cell* **169**, 326–337.e12 (2017).
60. P. C. He, C. He, m6A RNA methylation: From mechanisms to therapeutic potential. *EMBO J.* **40**, e105977 (2021).
61. S. Ke, A. Pandya-Jones, Y. Saito, J. J. Fak, C. B. Vågbø, S. Geula, J. H. Hanna, D. L. Black, J. E. Darnell, R. B. Darnell, m^{6}A mRNA modifications are deposited in nascent pre-mRNA and are not required for splicing but do specify cytoplasmic turnover. *Genes Dev.* **31**, 990–1006 (2017).
62. L. Arribas-Hernández, S. Rennie, T. Köster, C. Porcelli, M. Lewinski, D. Staiger, R. Andersson, P. Brodersen, Principles of mRNA targeting via the Arabidopsis m^{6}A-binding protein ECT2. *eLife* **10**, e72375 (2021).
63. D. Dominissini, S. Moshitch-Moshkovitz, M. Salmon-Divon, N. Amariglio, G. Rechavi, Transcriptome-wide mapping of N^6-methyladenosine by m^{6}A-seq based on immunocapturing and massively parallel sequencing. *Nat. Protoc.* **8**, 176–189 (2013).
64. L. Wang, E. Y. Kim, J. Cho, High-throughput profiling of extrachromosomal linear DNAs of long terminal repeat retrotransposons by ALE-seq. *Methods Mol. Biol.*, 103–110 (2021).
65. Z. Lei, E. Kim, J. Cho, Enrichment of cytoplasmic RNA granules from Arabidopsis seedlings. *Bio Protoc.* **11**, e4212 (2021).
66. J. Liu, L. Feng, X. Gu, X. Deng, Q. Qiu, Q. Li, Y. Zhang, M. Wang, Y. Deng, E. Wang, Y. He, I. Bäurle, J. Li, X. Cao, Z. He, An H3K27me3 demethylase-HSFA2 regulatory loop orchestrates transgenerational thermomemory in Arabidopsis. *Cell Res.* **29**, 379–390 (2019).
67. A. M. Bolger, M. Lohse, B. Usadel, Trimmomatic: A flexible trimmer for Illumina sequence data. *Bioinformatics* **30**, 2114–2120 (2014).
68. D. Kim, B. Langmead, S. L. Salzberg, HISAT: A fast spliced aligner with low memory requirements. *Nat. Methods* **12**, 357–360 (2015).
69. M. Pertea, G. M. Pertea, C. M. Antonescu, T.-C. Chang, J. T. Mendell, S. L. Salzberg, StringTie enables improved reconstruction of a transcriptome from RNA-seq reads. *Nat. Biotechnol.* **33**, 290–295 (2015).
70. J. T. Robinson, H. Thorvaldsdottir, W. Winckler, M. Guttman, E. S. Lander, G. Getz, J. P. Mesirov, Integrative genomics viewer. *Nat. Biotechnol.* **29**, 24–26 (2011).
71. Y. Zhang, T. Liu, C. A. Meyer, J. Eeckhoute, D. S. Johnson, B. E. Bernstein, C. Nusbaum, R. M. Myers, M. Brown, W. Li, X. S. Liu, Model-based analysis of ChIP-Seq (MACS). *Genome Biol.* **9**, R137 (2008).
72. H. Li, Minimap2: Pairwise alignment for nucleotide sequences. *Bioinformatics* **34**, 3094–3100 (2018).
73. J. Gleeson, A. Leger, Y. D. J. Prawer, T. A. Lane, P. J. Harrison, W. Haerty, M. B. Clark, Accurate expression quantification from nanopore direct RNA sequencing with NanoCount. *Nucleic Acids Res.* **50**, e19–e19 (2022).
74. X. Cui, Z. Wei, L. Zhang, H. Liu, L. Sun, S.-W. Zhang, Y. Huang, J. Meng, Guitar: An R/bioconductor package for gene annotation guided transcriptomic analysis of RNA-related genomic features. *Biomed. Res. Int.* **2016**, 1–8 (2016).
75. J. S. Harrison, E. M. Cornett, D. Goldfarb, P. A. DaRosa, Z. M. Li, F. Yan, B. M. Dickson, A. H. Guo, D. V. Cantu, L. Kaustov, P. J. Brown, C. H. Arrowsmith, D. A. Erie, M. B. Major, R. E. Klevit, K. Krajewski, B. Kuhlman, B. D. Strahl, S. B. Rothbart, Hemi-methylated DNA regulates DNA methylation inheritance through allosteric activation of H3 ubiquitylation by UHRF1. *eLife* **5**, e17101 (2016).
76. L. Wang, Zenodo, 10.5281/ZENODO.7969237.

Acknowledgments: We thank the Core Facility Center of CAS Center for Excellence in Molecular Plant Sciences for technical support with confocal microscopy. **Funding:** This work was supported by the grants listed as follows: Chinese Academy of Sciences Strategic Priority Research Program, XDB27030209 (J.C.); National Natural Science Foundation of China, 31970518 (J.C.), 32150610473 (J.C.), and 32111540256 (J.C.); and Natural Science Foundation of Shanghai, 22ZR1469100 (J.C.). **Author contributions:** Conceptualization: W.F. and J. Cho. Methodology: W.F., L.W., Z.L., H.L., J. Chu, M.Y., and Y.W. Investigation: W.F., L.W., Z.L., H.L., J. Chu, H.W., J.Y., and J. Cho. Visualization: L.W. and J. Cho. Supervision: J. Cho. Writing—original draft: W.F., L.W., and J. Cho. Writing—review and editing: J. Cho. **Competing interests:** The authors declare that they have no competing interests. **Data and materials availability:** All data needed to evaluate the conclusions in the paper are present in the paper and/or the Supplementary Materials. The NGS data that support the findings of this study have been deposited in SRA repository with the accession codes PRJNA873867 and summarized in table S4. The analyses were performed using the standard codes instructed by the tools described in Materials and Methods, and the custom codes used in this study are deposited in GitHub (https://github.com/JungnamChoLab) and Zenodo (*76*).

Submitted 14 October 2022
Accepted 30 October 2023
Published 29 November 2023
10.1126/sciadv.adf3292